Neurons derived from individual early Alzheimer's disease patients reflect clinical vulnerability

Bryan Ng[1], Helen Rowland[2], Tina Wei[3], Kanisa Arunasalam[3], Emma Mee Hayes[3], Ivan Koychev[2], Anne Hedegaard[2,14], Elena M. Ribe[2], Dennis Chan[4,15], Tharani Chessell[5], Dominic ffytche[6], Roger N. Gunn[7], Ece Kocagoncu[8], Jennifer Lawson[2], Paresh Malhotra[9], Basil H. Ridha[10], James B. Rowe[8], Alan J. Thomas[11], Giovanna Zamboni[12,16], Noel Buckley[2], Zameel M. Cader[3]*, Simon Lovestone[2,13]* and Richard Wade-Martins[1]*

Affiliations

[1] Department of Physiology Anatomy and Genetics, Kavli Institute for Nanoscience Discovery, University of Oxford, South Parks Road, Oxford OX1 3QU, United Kingdom

[2] Department of Psychiatry, University of Oxford, Headington, Oxford OX3 7JX, United Kingdom

[3] Weatherall Institute of Molecular Medicine, Nuffield Department of Clinical Neurosciences, Headington, University of Oxford, Oxford OX3 9DS, United Kingdom

[4] Department of Clinical Neurosciences, University of Cambridge, Cambridge, United Kingdom

[5] Neuroscience, Innovative Medicines and Early Development, AstraZeneca AKB, Granta Park, Cambridge, CB21 6GH, United Kingdom

[6] Department of Old Age Psychiatry, Institute of Psychiatry, Psychology and Neuroscience, Kings College London, SE5 8AF, United Kingdom

[7] Invicro & Department of Brain Sciences, Burlington Danes Building, Imperial College London, Hammersmith Hospital, Du Cane Road, London, W12 0NN, United Kingdom

[8] Medical Research Council Cognition and Brain Sciences Unit, Department of Clinical Neurosciences and Cambridge University Hospitals NHS Trust, University of Cambridge, Cambridge, United Kingdom

[9] Department of Brain Sciences, Imperial College London, Charing Cross Campus, London W6 8RP, United Kingdom

[10] Dementia Research Centre, UCL Institute of Neurology, Queen Square, London, WC1N 3BG, United Kingdom

[11] Translational and Clinical Research Institute, Newcastle University, Newcastle, United Kingdom

[12] Nuffield Department of Clinical Neurosciences, Headington, University of Oxford, Oxford OX3 9DS, United Kingdom

[13] Janssen Medical (UK) Ltd, High Wycombe, United Kingdom

[14] Current address: Sir William Dunn School of Pathology, University of Oxford, South Parks Road, Oxford OX1 3RE, United Kingdom

[15] Current address: Institute of Cognitive Neuroscience, University College London, London, United Kingdom

[16] Current address: Department of Biomedical, Metabolic, and Neural Science, University of Modena and Reggio Emilia, Modena Italy

*: Corresponding authors:

richard.wade-martins@dpag.ox.ac.uk

simon.lovestone@psych.ox.ac.uk

zameel.cader@ndcn.ox.ax.uk

Abstract

Modelling sporadic Alzheimer's disease (sAD) with patient-derived induced pluripotent stem cells (iPSCs) is challenging yet remains an important step in understanding the disease. Here we report a novel approach of sAD modelling with patient iPSC-derived neurons by integrating cellular and clinical phenotypes from individual early symptomatic sAD patients. We establish a correlation between cellular vulnerability to extrinsic amyloid-β *in vitro* measured by synapse loss with clinical vulnerability to amyloid-β burden *in vivo* measured by cognitive decline and brain activity levels. Our findings indicate that patient iPSC-derived neurons not only preserve some pathological phenotypes of disease measured in the people they were derived from, but also preserve, from people to cells, the impact of those pathological phenotypes on function. Cellular models that reflect an individual's in-life clinical vulnerability thus represent a tractable method of sAD modelling using clinical data in combination with cellular phenotypes.

Introduction

Alzheimer's disease (AD) is the most common age-related neurodegenerative disease and cause for dementia, estimated to affect close to 50 million people in 2015 worldwide with cases predicted to almost double every 20 years[1]. Autosomal dominant mutations in the Amyloid Precursor Protein gene (*APP*) or genes encoding the APP proteolytic enzymes Presenilins 1 and 2 (*PSEN1*, *PSEN2*) are causative of early onset familial AD (fAD). Largely based on insights from fAD, amyloid-β (Aβ) generation, metabolism or clearance is thought to underlie the pathogenesis of late onset forms of sAD. The wealth of evidence supporting this hypothesis has driven most drug development programs to date. However, it is also apparent that whilst amyloid-related features predict clinical outcomes, this relationship shows very considerable inter-individual variation[2]. Some individuals show evidence of extensive amyloid pathology

yet little apparent clinical impairment, and others have a relatively low amyloid burden in the context of moderately advanced dementia. Transgenic rodent models utilising human fAD gene mutations[3] have been extensively used to model various aspects of APP/Aβ pathobiology but have not proved useful in exploring the mechanisms whereby this pathobiology affects disease pathogenesis and, as a consequence, we have no effective preclinical model of sAD.

The advent of induced pluripotent stem cell (iPSC) technologies[4] making it possible to derive patient-specific cell lines capable of differentiating into various cell types, raises the potential of human cellular models of disease. Although fAD iPSC-derived cells exhibit pathological phenotypes *in vitro*, these are most obvious in APP related phenotypes such as a production of an increased ratio of $A\beta_{1\text{-}42}$ to $A\beta_{1\text{-}40}$ peptides, whereas sAD iPSC-derived cells typically do not share the same phenotypes [5–7]. Recently however, iPSC-derived neurons were shown to display features *in vitro* that reflect analogous features from post-mortem material from the same individuals – including congruence in gene expression profiles and some phenotypes related to both Aβ and tau pathologies[8]. This raises the possibility of using individual cell models of disease to explore pathogenesis.

Results

We set out to ask whether the heterogeneity of sAD patients could be accurately reflected in iPSC models by comparing clinical outcomes *in vivo* with patient-derived neuronal phenotypes *in vitro*. We asked specifically whether clinical vulnerability in the presence of Aβ burden in the brain can be reflected by Aβ-induced cellular vulnerability in neurons derived from the same patients. In this study, we tapped into the comprehensive clinical datasets of the Deep and Frequent Phenotyping (DFP) pilot cohort (Koychev et al.[9] and Supplementary Table 1) from which we generated thirteen sAD iPSC lines to use in our experiments (Supplementary

Fig. 1). Previously, the DFP study has highlighted the heterogeneity of disease, as have many others; showing, for example, a statistical correlation between amyloid burden measured by both positron emission tomography (PET) and cerebrospinal fluid (CSF) measures and clinical outcomes but also a very considerable inter-individual variation in the impact of that amyloid pathology[10].

To understand if patient-derived iPSC models recapitulate the in-life clinical measures of their donors, we first differentiated all thirteen iPSC lines in parallel into cortical neurons in monoculture (Extended Data Fig. 1a) and showed that $A\beta_{1-42}$ levels in the conditioned media correlate significantly and *negatively* with the same pathological Aβ species in the CSF from the patient donors (Fig. 1a). In other words, patient-derived neurons which secret greater levels of $A\beta_{1-42}$ were generated from donors with lower CSF $A\beta_{1-42}$ levels, a characteristic phenomenon of AD patients due to the sequestration of $A\beta_{1-42}$ in non-soluble cortical amyloid plaques[11]. Importantly, this relationship was not replicated in either $A\beta_{1-38}$ or $A\beta_{1-40}$ peptide comparisons. This result provides further evidence that patient-derived neurons reflect the pathological features *in vivo* of that patient. We next went on to examine patient-specific cellular vulnerability to Aβ *in vitro*.

Dysregulation, and eventually loss, of synapses is one of the earliest pathological phenotypes of AD and leads to cognitive decline and memory loss[12,13]. Electrophysiology, in particular magnetoencephalography (MEG), is thought to be a surrogate of synaptic dysregulation and loss and hence provides an opportunity to explore whether the individual impact of sAD pathology on synaptic health in people *in vivo* is reflected in their cells *in vitro*. We therefore sought to investigate synapse loss in response to Aβ insults *in vitro;* iPSC lines were again differentiated in parallel into cortical neurons, this time plated in co-culture with rat cortical

astrocytes (Extended Data Fig. 1a, 1b). On Day 80 of the differentiation, we treated the neurons with extrinsic Aβ insults, namely $A\beta_{1-42}$ oligomers (10 μM), $A\beta_{25-35}$ oligomers (20 μM) or human AD brain homogenate (25% v/v), or relevant controls, before paraformaldehyde fixation. We then performed immunocytochemistry on neurons with presynaptic (SYNAPSIN I/II), postsynaptic (HOMER1) and dendritic (MAP2) markers before we conducted automated imaging on an Opera Phenix high-content confocal microscope.

The patient-derived cortical neurons showed different levels of synaptic density and the Aβ insults led to varying degrees of synapse loss among the patient lines, from the most resilient to the most vulnerable (Fig. 1b and Extended Data Fig. 1c, 2a). All neurons displayed functional activity by firing action potentials on Day 80 of neuronal differentiation (Extended Data Fig. 1d). The synapse loss datasets demonstrated good reproducibility over three repeat independent iPSC differentiations. By comparing the extents of synapse loss between differentiation repeats, we confirmed that the specific levels of vulnerability in each line of iPSC-derived neurons in response to Aβ insults remained consistent across all differentiation repeats (Fig. 1c and Extended Data Fig. 3a, 3c). Importantly, similar patient line-specific vulnerability measured by synapse loss was also consistent across the different Aβ insults used, especially between $A\beta_{1-42}$ and $A\beta_{25-35}$ oligomers where there is a significant and positive correlation (Extended Data Fig. 3b). A positive correlation was also observed across differentiation repeats when the neurons were treated with AD brain homogenate (Extended Data Fig. 3a, 3c). The synapse loss data indicated that the degree of synapse loss due to the exposure to extrinsic Aβ in functional cortical neurons is patient-specific and cell-autonomous.

Next, we explored if the levels of synaptic vulnerability to Aβ insults in the patient-derived neurons *in vitro* was reflected in their own synaptic and cognitive outcomes, the ultimate

clinical reflection of synaptic function. Global MEG recordings and cognitive decline measured by Mini Mental State Examination (MMSE) score loss rate (Supplementary Table 1) were adjusted as a function of the patients' individual levels of Aβ burden as described in the Methods. This yielded a personal clinical vulnerability quotient representing the synaptic and cognitive response as a function of amyloid pathological load per individual, ranging between 0 and 1 with the value of 1 being the most vulnerable in this cohort.

Discussion

Using this analysis, we found that the amount of synapse loss in patient-derived neurons caused by Aβ insults *in vitro* reflects the personal clinical vulnerability to Aβ burden *in vivo*, whether measured by the surrogate measure of synaptic number and function – MEG - or by cognitive decline, the core clinical manifestation of synaptic loss. Specifically, we observed a positive correlation between the percentage of synapse loss caused by both $A\beta_{1\text{-}42}$ and $A\beta_{25\text{-}35}$ oligomers and clinical vulnerability quotients, demonstrating that greater cellular vulnerability correlates significantly with greater clinical vulnerability in these patients (Fig. 2). Synapse loss due to the exposure to human AD brain homogenate resulted in similar correlation with clinical vulnerability quotients (Extended Data Fig. 4a). Additionally, the differences in synapse loss in the patient-derived neurons could not be explained by their *APOE* variants (Extended Data Fig. 2b). In conclusion, we show here that neurons derived from sAD patients retain the same individual vulnerability to Aβ that the person from whom they were derived, showed using both biomarkers and clinical measures that reflect the synaptic phenotypes measured *in vitro*.

In this study, we demonstrate for the first time that cellular vulnerability to Aβ insults *in vitro* reflects clinical vulnerability to Aβ burden *in vivo*, specifically in people living with AD dementia, by establishing the correlation between synapse loss in individual sAD patient-

derived neurons and their clinical outcomes. This approach of integrating clinical in-life data with disease modelling in the laboratory presents a tractable method of sAD modelling with iPSCs.

Decline in cognition estimated from time since onset and current cognitive score, and 'brain activity' assessed using MEG were selected as clinical outcomes likely to be reflections of synaptic health and so broadly analogous to the synaptic loss data we measured *in vitro*. In both cases we establish an individualized clinical outcome as a function of 'amyloid burden' using CSF Aβ as a measure of that burden. We report here that, indeed, cognitive decline as a function of Aβ burden correlates with more severe Aβ-driven synapse loss in the patient-derived neurons. Interestingly, we did not consistently observe such correlations when we corrected the clinical outcomes for amyloid PET (Extended Data Fig. 4b) perhaps suggesting that CSF Aβ is a more direct reflection of the pathological insult in AD than the aggregations of fibrillated Aβ in plaques measured by PET. Further, larger studies will be needed to substantiate this tentative but potentially important, observation, which has been the subject of much debate in the field. Although it has been known that synapse loss correlates with cognitive decline in AD[13,14], and that MEG identifies neurophysiological changes that are specific to AD, it remains unclear how different brain MEG signals change at different stages of AD progression[15,16]. We find a clear correlation between *greater* brain activity levels measured by MEG correlating with more severe Aβ-driven synapse loss in the patient-derived neurons. This apparently counterintuitive observation is in fact in line with a considerable amount of evidence for hyperexcitability in the early phases of AD. Neurons exhibit hyperactivation particularly during the mild cognitive impairment stage before hypoactivation as disease progresses[17,18], and hyperexcitability leading to seizure activity is increased in AD, perhaps as a function of amyloid related pathology[19]. Indeed, recent preclinical evidence

suggests that such excitability and seizure activity might accelerate the progression of tau related pathology and hence actually be a target for therapy[20].

It has recently been shown that several measures of secreted Aβ peptides in iPSC-derived cortical neurons from AD patients reflect the extent of Aβ neuropathology of their donors[8]. We extend that work on neuropathological findings to in-life clinical measurements by showing that the levels of $A\beta_{1\text{-}42}$ secreted from patient-derived neurons correlate with the levels of the same pathological Aβ species in the patient CSF samples (Fig. 1a). However, we have now shown that not only is there a correlation between cellular phenotypes and analogous phenotypes in post-mortem brain and in patients, but that the functional consequences of those phenotypes – the response to Aβ as well as the amount of Aβ – are preserved in the cells.

In conclusion, we reveal that cellular vulnerability reflects clinical vulnerability to Aβ in sAD by modelling with patient iPSC-derived neurons and integrating cellular and clinical data from a highly-phenotyped cohort. We first demonstrated the correlation between levels of $A\beta_{1\text{-}42}$ secreted from patient iPSC-derived cortical neurons and the levels of the same pathological Aβ species in the patient CSF samples, and then demonstrated Aβ-driven synapse loss in iPSC-derived neurons reflects relevant clinical outcomes as a function of Aβ burden in the brain. This work establishes the feasibility of modelling in-life sAD clinical phenotypes with patient iPSC-derived neurons. Beyond that, as we can model inter-individual variability in clinical response to Aβ insult in an individual's own iPSC derived neurons in vitro, this raises the potential for interrogating mechanisms, and identifying targets for precision therapy in human cell models.

Methods

All reagents were purchased from Sigma unless stated otherwise.

DFP cohort pilot study and clinical data

The DFP cohort pilot study protocol was detailed in Koychev et al. (2019)[9] and a subset of the comprehensive clinical data and study participants (13 early symptomatic AD cases) was used for the analyses. The AD patients were aged between 56 and 82 years old and 5/13 were female. Briefly for the study protocol, both amyloid PET imaging with [^{18}F] AV45 (0–60 min, 150 ± 24 MBq) and MEG recordings were conducted once in 9/13 and 7/13 of the pilot study participants respectively. Global efficiency metric from the γ-band (32-100 Hz) of the MEG raw data was used for analysis as it is the oscillation range linked to cognitive function and local connectivity[21]. Lumbar puncture was performed over two visits 169 days apart in 11/13 of the study participants for CSF collection and $A\beta_{1\text{-}42}$ peptide concentration was quantified via electrochemiluminescence in 96-well plates from Meso Scale Discovery (Aβ peptide panel 1 with 6E10 antibody), before deriving the average values from the two visits for downstream analyses. All pilot study participants underwent cognitive testing including a Mini Mental State Examination (MMSE; Mean = 25.2) and a MMSE score loss rate measuring cognitive decline was derived by dividing the MMSE score differences between the baseline visit and symptom onset with the time difference in days. We then calculated a 'clinical vulnerability quotient' ranging from 0 (least vulnerable or most resistant) to 1 (most vulnerable, least resistant) by deriving a clinical outcome as a function of that individual's CSF $A\beta_{1\text{-}42}$ levels (Fig. 2) or PET standard uptake value ratios (Extended Data Fig. 4b).

Generation of AD patient-derived iPSC lines from blood samples

Blood samples (8 ml) were remixed via gently inversion and centrifuged at 1800 g/20 min with brakeless deceleration. The plasma portion was removed, taking care not to disturb the whitish phase ring containing the peripheral blood mononuclear cells (PBMC). PBMC were diluted to 40 ml using PBS (Thermo) (added dropwise to prevent osmotic shock) and centrifuged at 300 g/15 min. Cells were counted and plated at 5 x 10^6/ml in Expansion I medium which consists of StemSpan SFEM (Stem Cell Technologies) supplemented with lipid concentrate (1 %. Gibco), dexamethasone (1 µM), IGF-1 (40 ng/ml, R&D Systems), IL-3 (10 ng/ml, R&D Systems), EPO (2 U/ml, R&D Systems) and SCF (100 ng/ml R&D Systems). The remaining wells were filled with PBS to maintain a humid atmosphere (continued throughout all expansion and reprogramming steps). From DIV-1 to DIV-6, a 50 % media change (Expansion I medium) was performed. Erythroblasts should appear ~ DIV-5.

To purify the erythroblast population, 4 ml Percoll was first added to a 15 ml tube. The wells were washed with DMEM (used for all washing steps) before a maximum of 8 ml cell solution was slowly trickled onto the Percoll solution to collect erythroblasts. The solution was centrifuged at 1000 g/20 min with brakeless deceleration. The supernatant above the phase ring was transferred to a new tube and centrifuged at 300 g/5 min and washed twice to remove the Percoll. Purified erythroblasts were plated at 1-1.5 x 10^6/ml in Expansion II medium which has the same constituents as Expansion I medium except IL-3. On DIV-8/9, erythroblasts were collected, centrifuged at 200 g/5 min, resuspended in Expansion II medium, and plated at 1-1.5 x 10^6/ml to prevent cells differentiating down the erythroid lineage.

Before reprogramming erythroblasts to iPSCs, each well of a six-well plate was coated with 1 ml of 0.1% gelatine at 37°C for > 20 minutes. Mitomycin-C treated CF1 Mouse Embryonic Fibroblasts (MEF) were thawed and transferred to a tube containing 34 ml MEF medium which

consists of Advanced DMEM supplemented with fetal calf seum (10 %), GlutaMAX (1 %) and 2-mercaptoethanol (0.1 %) all purchased from Life Technologies. The gelatine was aspirated from the wells and two ml of MEF suspension were added per well. Plates were incubated overnight at 37°C before erythroblasts were plated after undergoing viral transduction.

Erythroblasts were collected and centrifuged at 200 g/5 min when they were ready to be infected with Sendai viruses expressing Yamanaka factors. The pellet was resuspended in Expansion II media. 1.5 x 10^5 cells were collected and made up to 200 µl in Expansion II media. An aliquot from the CytoTune™-iPS 2.0 Sendai Reprogramming Kit (Thermo) was thawed on ice, mixed with 150 µl Expansion II media and added to cell suspension. The entire suspension was transferred to a well in a 24-well plate. Viral supernatant was removed 23 h later by collecting cells and centrifuging at 300 g/4 min. The pellet was resuspended in Expansion II media and transferred to a well in a 24-well plate before incubating for 48 h.

Finally, MEF medium was removed from feeder plates which were washed with PBS before 1 ml of Expansion II media was added. The transduced erythroblasts were collected, centrifuged at 300 g/4 minutes, and resuspended in Expansion II media. The cells were plated at a range of densities (1.5 - 4.5 x 10^4/ml) which yielded approximately eight to twelve clones but allowed the clones to grow large enough for picking without overcrowding. A 50% media change was performed on the following days with the following media – DIV-5 (Expansion II media), DIV-7/8 (hES medium which consists of KnockOut DMEM supplemented with 20 % KnockOut Serum Replacement, 1 % GlutaMAX, 1 % non-essential amino acids, 0.1 % 2-mercaptoethanol and 10 ng/ml BFGF) and DIV-10 (Conditioned Medium derived from MEF culture with hES medium). Clones appeared ~ DIV-15 and were picked ~ DIV-22. If clones did not appear by DIV-40, the line was deemed to have failed to reprogramme. Colonies that displayed

embryonic stem cell-like morphology were selected via manual picking. All iPSC lines used in this study express pluripotency markers Tra-1-60 and NANOG measured by fluorescence-activated cell sorting.

Maintaining iPSC culture and differentiation into iPSC-derived cortical neurons

iPSC culture was maintained by growing the cells on Matrigel matrix (Corning) and feeding with mTeSR™ medium (STEMCELL technologies) which was replaced daily. We differentiated the iPSC lines into cortical neurons by overexpressing Neurogenin-2 (*Ngn2*)[22]. All 13 iPSC lines were infected with lentivirus carrying the plasmids for *Ngn2* overexpression, before we plated the cells onto poly-ornithine (100 µg/ml) plus laminin (10 µg/ml) coated cell culture plates at 60,000 cells/cm^2 (double for several lines which did not grow well) in mTeSR™ medium (STEMCELL Technologies) supplemented with Y-27632 (Tocris) at 10 µM on Day 0. The mTeSR™ medium was replaced with Neurobasal™ medium (Gibco) supplemented with B27™ (Thermo), GlutaMAX™ (Gibco), Penicillin-Streptomycin (Gibco), neurotrophin-3 (10 ng/ml). BDNF (10 ng/ml, Peprotech), doxycycline (1 µg/ml), laminin (200 ng/ml) and ascorbic acid (200 µM) five hours after plating. Subsequently, the cell culture medium was further supplemented with puromycin (1.5 µg/ml) on Day 2 only.

The cells underwent the only and final passage on Day 4 with Accutase™ and were plated at 25,000 cells/cm^2 onto a confluent layer of rat cortical astrocytes (Thermo Fisher) in half-area 96-well plates. Half-feeding took place twice per week from Day 4 onwards with the abovementioned B27-containing medium. Finally, we also supplemented the medium with Ara-C (100 nM final concentration) on Day 10, 20, 40 and 60.

Multi-electrode array (MEA)

The iPSCs were seeded directly onto the MEA plates, and 30,000 rat cortical astrocytes were seeded into each well of the MEA plates on Day 5 of the differentiation. From Day 45 onwards of the cortical neuron differentiation, 2-min long recordings were taken after 5 mins plate settling time on the MEA reader regularly over time (Axion Biosystems, Maestro) with AxIS software v2.4.2.13 (Axion Biosystems). The plate was kept at 37°C while recordings were taken. The raw recording files were then extracted with AxIS software (Axion Biosystems) and processed with custom script in MATLAB (version R2020b).

Meso Scale Discovery (MSD) immunoassay of Aβ peptides

The iPSC derived neurons were grown as described previously without the Day 4 passage onto rat astrocytes until Day 40. Cell conditioned media was collected after 48 hours and stored at -80 °C. Cells were washed once with PBS, and M-PER™ (Thermo) added for 20 min on ice. Cell suspension was centrifuged at 14,000 g for 10 min at 4°C. The supernatant was collected, and protein concentration was quantified by BCA assay (Thermo). Measurement of Aβ38, Aβ40, Aβ42 was measured by electrochemiluminescence using MSD V-PLEX Aβ peptide panel (6E10), which was carried out according to manufacturer's protocol. Cell media samples were run in triplicate, with 25 µg of each cell lysate run in duplicate and kept on a plate shaker covered with a plate seal at room temperature during incubation. The MSD Workbench 4.0 software (MSD) was used to analyse Aβ levels. Conditioned media samples were normalised to the average of total protein concentration in the lysate.

Oligomerisation of Aβ peptides and treatment in neuronal culture

Both lyophilised $A\beta_{1-42}$ and treatment control scrambled $A\beta_{1-42}$ peptides (Bachem, H-1368 and H-7406) were resuspended to 1 mM in Hexafluoro-2-propanol (HFIP). The tubes were vortexed and left sitting at room temperature for 30 min, before they were aliquoted and dried

in a Speed-Vac concentrator for 30 min. We kept the Aβ film at -80 °C. To oligomerise the $A\beta_{1-42}$ peptides, we first resuspended the Aβ film in DMSO to 5 mM before sonicating in water bath for 10 min. PBS was then added to result in 100 µM solution and the tubes were left stationary at 4 °C for 24 h. Just before treating the cells with Aβ oligomers, the solution was centrifuged at 14,000 g for 10 min at 4 °C to remove any precipitate/fibrils.

Both lyophilised $A\beta_{25-35}$ and treatment control $A\beta_{35-25}$ peptides (Bachem, H-1192 and H-2964) were resuspended to 2 mg/ml in deionised water and vortexed before incubating at 37 °C for 2 h for oligomerisation. The vial was then aliquoted and frozen at -80 °C.

The iPSC-derived neurons were incubated with Aβ oligomers for 24 h before paraformaldehyde fixation.

Human AD brain homogenate extraction

The extraction protocol was modified from the work of Jin *et al.*[23]. We sourced the post-mortem frozen frontal cortices from two AD patients (Patient #1: 73yo, female, Braak stage VI, 75 h post-mortem delay; Patient #2: 81yo, male, Braak stage VI, 26 h post-mortem delay) from the Oxford Brain Bank. We first thawed the brain tissues on ice prior to homogenisation with Dounce homogenisers for 25 strokes in cold artificial CSF (aCSF: 124 mM NaCl, 2.8 mM KCl, 1.25 mM NaH_2PO_4 and 26 mM $NaHCO_3$, pH = 7.4) with a ratio of 1 g of tissue to 4 mL of aCSF supplemented with a panel of protease inhibitors (5 mM EDTA, 1 mM EGTA, 5 ug/ml leupeptin, 5 µg/ml aprotinin. 2 µg/ml pepstatin, 120 µg/ml Pefabloc and 5 mM NaF). The homogenisation was followed by centrifugation at 200,000 g for 110 min at 4 °C and the supernatant was transferred into a Slide-A-Lyzer™ G2 Dialysis Cassettes 2K MWCO in 100

times volumn of aCSF without protease inhibitors for 72 h. The aCSF was replaced every 24 h and the resultant aliquots were frozen at -80 °C.

The iPSC-derived neurons were incubated with either 25 % AD brain homogenate (1:1 mixture from the two cortices) or aCSF without protease inhibitors as the treatment control in the cell culture medium (v/v) for 72 h at 37°C before paraformaldehyde fixation.

Immunocytochemistry

Adherent neurons were fixed in 4 % paraformaldehyde for 5 min, followed by treating with 0.5% saponin in PBS for 20 min for permeabilisation. To block the samples, we treated the plates with 10% normal goat serum (NGS) with 0.01% tween-20 in PBS for 30 min. Primary antibodies were then left incubating with the samples at 4°C overnight with 1% NGS and 0.01% tween-20, before washing with PBS 3 times. Secondary antibodies were then applied in 1% NGS and 0.01% tween-20 at room temperature for 1 h before washing for another four times. The primary antibodies we used were: Guinea pig anti-SYNAPSIN I/II (Synaptic Systems, 1:500), rabbit anti-HOMER1 (Synaptic Systems, 1:500), chicken anti-MAP2 (Abcam, 1:1000), mouse anti-human nuclear antigen (Abcam, 1:200), rabbit anti-CUX2 (Abcam, 1:200) and rat anti-CTIP2 (Abcam, 1:500). The secondary antibodies we used were: Goat anti-guinea pig Dylight 488 (Abcam), goat anti-mouse Alexa Fluor 488, goat anti-rabbit Alexa Fluor 555, goat anti-chicken Alexa Fluor 555, goat anti-rabbit Alexa Fluor 647 and goat anti-rat Alexa Fluor 647 (Thermo) at 1:1000 dilution.

High-content imaging and analysis

Synapse: The 96-well plates were imaged on the Perkin Elmer Opera Phenix high-content imager. We captured 15 images per well with a 43X objective at +1 µm focus level with the

binning value of 1. We then analysed the image with the Harmony software v4.9 from Perkin Elmer with a customised pipeline. The MAP2-positive neurites were identified with 0.5 overall threshold as the region of interest and resized by expanding outwards by 5 px to cover synaptic signals which lay slightly above the MAP2 signals. Both presynaptic (SYNAPSIN I/II) and postsynaptic (HOMER1) signals were then identified with Method A of the "Find spots" function with threshold values of 0.17 and 0.14, respectively. We also filtered away the spots which were larger than 100 px^2. Finally, the synapses were ascertained by finding HOMER1 signals in the vicinity of SYNAPSIN I/II signal regions which had been resized by expanding outwards by 5 px. The absolute number of synapses was then normalised to the total MAP2-positive area to derive synaptic density which was used for all downstream analyses. All the values of synaptic density downregulation due to the Aβ extrinsic insults were then normalised to the corresponding treatment controls (e.g. $A\beta_{1\text{-}42}$ normalised to scrambled $A\beta_{1\text{-}42}$).

Cortical markers: We captured 15 images at -1, 0 and +1 and µm focus levels per well with a 20X objective and binning value of 2. We analysed the images on the same Harmony software by first identifying human nuclei among the co-culture with rat astrocytes and filtering away the nuclei with circularity less than 0.6. The percentage of cortical marker-positive cells was calculated by selecting the human nuclei with cortical marker mean signal intensity greater than a threshold which was determined as the mean intensity across all human nuclei. Finally, we derived relative cortical marker expression by normalising the percentage of cortical marker-positive neurons to the geometric mean across all thirteen patient neuronal lines.

Statistical analyses

All quantitative graphs and statistical analyses were performed in GraphPad Prism 9.2.0. For the correlation representations by simple linear regression line fittings, we reported Pearson's

coefficient of correlation and two-tailed p-values to indicate statistical significance. Kruskal-Wallis test was used for comparisons amongst the patient lines for synaptic density, cortical marker expression levels, synapse loss and *APOE* genotypes.

Data availability statement

The data that support the findings are presented in the figures or table included in the paper. More detailed raw data of the experiments are available from the corresponding authors upon reasonable request. The data from the DFP cohort can be requested via the DPUK online portal (https://www.dementiasplatform.uk/research-hub/data-portal).

Acknowledgements

We thank all participants of the Deep and Frequent Phenotyping pilot cohort for contributing clinical data and samples towards this study. We thank S Cowley, J Vowles and S Chintawar for technical assistance in characterising iPSC lines. This work was funded by a National Institute for Health Research (NIHR)-Medical Research Council (MRC) Dementias Platform UK (DPUK) Experimental Medicine Award and a NIHR-MRC DPUK Equipment Award. The Deep and Frequent Phenotyping clinical study is funded by the MRC. This project was supported by StemBANCC funding from the Innovative Medicines Initiative Joint Undertaking under Grant Agreement Number 115439, resources of which are composed of financial contribution from the European Union's Seventh Framework Programme (FP7/2007e2013) and EFPIA companies in kind contribution. The work was also supported by the NIHR Oxford Biomedical Research Centre. B.N. was supported by the National Science Scholarship by the Agency for Science, Technology and Research, Singapore. H.R. was supported by an Alzheimer's Research UK Thames Valley Network Pump Priming Award. I.K. received support through the Oxford Health Biomedical Research Centre, the MRC and

the NIHR. B.H.R. was supported by the NIHR Biomedical Research Centre (BRC) at UCLH and P.M. supported by the NIHR BRC at Imperial College London.

Author contributions

R.W.-M., Z.M.C. and S.L. conceived the study design. B.N., S.L. and R.W.-M. contributed to the experiment design. S.L. was the PI and D.C, T.C., D.f., R.N.G., E.K., J.L., P.M., B.H.R., J.B.R, A.J.T. and G.Z. contributed to the design and execution of the clinical study. B.N., H.R. and T.W. contributed materials for experiments, performed experiments, data acquisition, analysis, and presentation. K.A., E.M.H. and A.H. contributed to cell line generation, quality control and expansion. B.N., H.R., T.W., I.K., E.M.R., N.B., J.R., Z.M.C., S.L. and R.W.-M. contributed to data analysis and interpretation. E.M.R., N.B., Z.M.C, S.L. and R.W.-M. supervised the study. B.N. drafted the manuscript and B.N., I.K., S.L. and R.W.-M. edited the manuscript. R.W.-M. finalised the manuscript before all authors approved the final version of the manuscript.

Ethics statement

The DFP cohort study was approved by the London Central Research Ethics Committee, 14/LO/1467. The human iPSC lines used for this study were derived from human blood erythroblasts, (NHS Research Ethics Committee: 10/H0505/71) and were derived as part of the Innovative Medicine Initiative-EU sponsored StemBANCC consortium. Informed consent was obtained from all donors.

References

1. Prince, M. *et al.* World Alzheimer Report 2015: The Global Impact of Dementia - An analysis of prevalence, incidence, cost and trends. *Alzheimer's Dis. Int.* 84 (2015).

doi:10.1111/j.0963-7214.2004.00293.x

2. Doraiswamy, P. M. *et al.* Florbetapir F 18 amyloid PET and 36-month cognitive decline:a prospective multicenter study. *Mol. Psychiatry 2014 199* **19**, 1044–1051 (2014).

3. Tanzi, R. E. The genetics of Alzheimer disease. *Cold Spring Harb. Perspect. Med.* **2**, (2012).

4. Takahashi, K. & Yamanaka, S. Induction of pluripotent stem cells from mouse embryonic and adult fibroblast cultures by defined factors. *Cell* **126**, 663–76 (2006).

5. Israel, M. A. *et al.* Probing sporadic and familial Alzheimer's disease using induced pluripotent stem cells. *Nature* **482**, 216–220 (2012).

6. Kondo, T. *et al.* Modeling Alzheimer's disease with iPSCs reveals stress phenotypes associated with intracellular Aβ and differential drug responsiveness. *Cell Stem Cell* **12**, 487–496 (2013).

7. Rowland, H. A., Hooper, N. M. & Kellett, K. A. B. Modelling Sporadic Alzheimer's Disease Using Induced Pluripotent Stem Cells. *Neurochem. Res. 2018 4312* **43**, 2179–2198 (2018).

8. Lagomarsino, V. N. *et al.* Stem cell-derived neurons reflect features of protein networks, neuropathology, and cognitive outcome of their aged human donors. *Neuron* (2021). doi:10.1016/J.NEURON.2021.08.003

9. Koychev, I. *et al.* Deep and Frequent Phenotyping study protocol: An observational study in prodromal Alzheimer's disease. *BMJ Open* **9**, e024498 (2019).

10. Koychev, I. *et al.* PET Tau and Amyloid-β Burden in Mild Alzheimer's Disease: Divergent Relationship with Age, Cognition, and Cerebrospinal Fluid Biomarkers. *J. Alzheimer's Dis.* **60**, 283–293 (2017).

11. R, M. *et al.* Reduction of beta-amyloid peptide42 in the cerebrospinal fluid of patients

with Alzheimer's disease. *Ann. Neurol.* **38**, 643–648 (1995).

12. Davies, C. A., Mann, D. M. A., Sumpter, P. Q. & Yates, P. O. A quantitative morphometric analysis of the neuronal and synaptic content of the frontal and temporal cortex in patients with Alzheimer's disease. *J. Neurol. Sci.* **78**, 151–164 (1987).
13. RD, T. *et al.* Physical basis of cognitive alterations in Alzheimer's disease: synapse loss is the major correlate of cognitive impairment. *Ann. Neurol.* **30**, 572–580 (1991).
14. Dickson, D. W. *et al.* Correlations of synaptic and pathological markers with cognition of the elderly. *Neurobiol. Aging* **16**, 285–298 (1995).
15. Ikeda, Y. *et al.* Spontaneous MEG activity of the cerebral cortex during eyes closed and open discriminates Alzheimer's disease from cognitively normal older adults. *Sci. Rep.* **10**, 1–9 (2020).
16. Mandal, P. K., Banerjee, A., Tripathi, M. & Sharma, A. A comprehensive review of magnetoencephalography (MEG) studies for brain functionality in healthy aging and Alzheimer's disease (AD). *Frontiers in Computational Neuroscience* **12**, 60 (2018).
17. O'Brien, J. L. *et al.* Longitudinal fMRI in elderly reveals loss of hippocampal activation with clinical decline. *Neurology* **74**, 1969–1976 (2010).
18. Dickerson, B. C. *et al.* Increased hippocampal activation in mild cognitive impairment compared to normal aging and AD. *Neurology* **65**, 404–411 (2005).
19. Romoli, M., Sen, A., Parnetti, L., Calabresi, P. & Costa, C. Amyloid-β: a potential link between epilepsy and cognitive decline. *Nat. Rev. Neurol. 2021 178* **17**, 469–485 (2021).
20. Alyenbaawi, H. *et al.* Seizures are a druggable mechanistic link between tbi and subsequent tauopathy. *Elife* **10**, 1–33 (2021).
21. Tallon-Baudry, C. & Bertrand, O. Oscillatory gamma activity in humans and its role in object representation. *Trends Cogn. Sci.* **3**, 151–162 (1999).
22. Zhang, Y. *et al.* Rapid single-step induction of functional neurons from human

pluripotent stem cells. *Neuron* **78**, 785–798 (2013).

23. Jin, M. *et al.* An in vitro paradigm to assess potential anti-Aβ antibodies for Alzheimer's disease. *Nat. Commun.* **9**, (2018).

Figure legends

Figure 1: Secreted Aβ levels correlated with CSF Aβ levels, and degrees of synapse loss due to Aβ insults showed different levels of vulnerability among patient-derived neurons.

(A) Pairwise comparisons between the levels of secreted Aβ species from the patient-derived neurons and the levels of the same Aβ species in the patient CSF. Error band: 95 % CI. N = 33 independent neuronal differentiation repeats per patient line.

(B) Representative immunofluorescence images from three selected patient lines ranging from the least to the most vulnerable to $A\beta_{1\text{-}42}$ oligomer insults relative to the scrambled peptide control treatment. The images are labelled with presynaptic (Synapsin I/II, green), postsynaptic (Homer1, red) and dendritic (MAP2, yellow) markers. White arrows indicate synapse examples with pre- and post-synaptic markers in apposition. Scale bar = 50 μm.

(C) Pairwise comparisons of the degrees of synapse loss between differentiation repeats, caused by either $A\beta_{1\text{-}42}$ or $A\beta_{25\text{-}35}$ oligomers. The same three selected patient lines from Fig. 1b are highlighted in the graphs.

Figure 2: Synapse loss due to Aβ insults in vitro reflects clinical vulnerability in the same patients to Aβ burden in vivo.

Pairwise correlations between the percentage of synapse loss and clinical vulnerability quotients. Each row denotes the type of oligomers used to induce synapse loss and each column

denotes the selected clinical outcomes which have been corrected for $A\beta_{1-42}$ concentration in the CSF. Error band: 95 % CI. N = 32 ($A\beta_{1-42}$ - MMSE score loss rate), 33 ($A\beta_{25-35}$ - MMSE score loss rate) and 18 (MEG) independent neuronal differentiation repeats per patient line.

Extended Data Figure 1: Characterisation of iPSC-derived cortical neurons.

(A) Schematic of the cortical neuron differentiation protocol over 80 days.

(B) Representative images of cortical markers from three patient lines ranging from the least to the most vulnerable to Aβ insults, as well as the quantification of relative expression levels across all patient lines. Scale bar = 100 µm. Mean ± SD. N = 3 independent neuronal differentiation repeats.

(C) Relative synaptic density across all patient-derived cortical neurons, normalised to the mean of synaptic density per neuronal differentiation. Mean ± SD. N = 3 independent neuronal differentiation repeats.

(D) Neuronal activity increase over time measured by multi-electrode array (MEA). The figure plots medians of extracellular firing rate in Hz of cortical neurons between day 40 to day 85 post plating on the MEA plate. The small dots are the raw data points recorded. Each raw recording has the length of 2 min from which median was calculated.

Extended Data Figure 2: Varying levels of synapse loss caused by Aβ insults.

(A) Percentage of synapse loss caused by $A\beta_{1-42}$ oligomers, $A\beta_{25-35}$ oligomers and AD brain homogenate across all patient lines normalised to their respective treatment controls. Mean ± SD. N = 3 independent neuronal differentiation repeats.

(B) Box plots (centre line, median; box limits, interquartile range; whiskers, data range; points, all data points) showing the percentage of synapse loss caused by $A\beta_{1-42}$ oligomers, $A\beta_{25-35}$

oligomers and AD brain homogenate with patients distinguished by their *APOE* variant genotypes. N = 9 (ε4-), 20 (ε3/ε4) and 9 (ε4/ε4) independent neuronal differentiation repeats per patient line.

Extended Data Figure 3: Good reproducibility of the synapse loss data across neuronal differentiation repeats indicates cell-autonomous vulnerability to Aβ insults.

(A) Pairwise comparisons on the degrees of synapse loss between differentiation repeats caused by AD brain homogenate. The same three selected patient lines from Fig. 1a are highlighted in the graphs.

(B) Pairwise comparison on the degrees of synapse loss caused by either $A\beta_{1\text{-}42}$ or $A\beta_{25\text{-}35}$ oligomers. The zones where the same three selected patient lines from Fig. 1a can be found are circled in the graphs.

(C) Breakdown of individual pairwise comparisons on the degrees of synapse loss between differentiation repeats summarised in Fig 2b. Each row denotes the two differentiation repeats in question and each column denotes the Aβ insult used to induce synapse loss.

Extended Data Figure 4: Additional pairwise correlations between the synapse loss data and clinical vulnerability quotients.

(A) Pairwise correlations between the percentage of synapse loss caused by AD brain homogenate *in vitro* and clinical vulnerability quotients on MEG and MMSE outcomes *in vivo*. Each column denotes the selected clinical outcomes and each raw denotes the Aβ biomarker to which the selected clinical outcomes were normalised to. Error band: 95 % CI. N = 33 (MMSE score loss rate/CSF $A\beta_{1\text{-}42}$), 27 (MMSE score loss rate/PET), and 18 (MEG/CSF $A\beta_{1\text{-}42}$) and 21 (MEG/PET) independent neuronal differentiation repeats per patient line.

(B) Pairwise correlations between the percentage of synapse loss caused by either $A\beta_{1-42}$ or $A\beta_{25-35}$ oligomers *in vitro* and clinical vulnerability quotients on MEG and MMSE outcomes *in vivo* corrected for amyloid PET SUVR in the brain. Each row denotes the type of oligomers used to induce synapse loss and each column denotes the selected clinical outcomes. Error band: 95 % CI. N = 27 (MMSE score loss rate) and 21 (MEG) independent neuronal differentiation repeats per patient line.

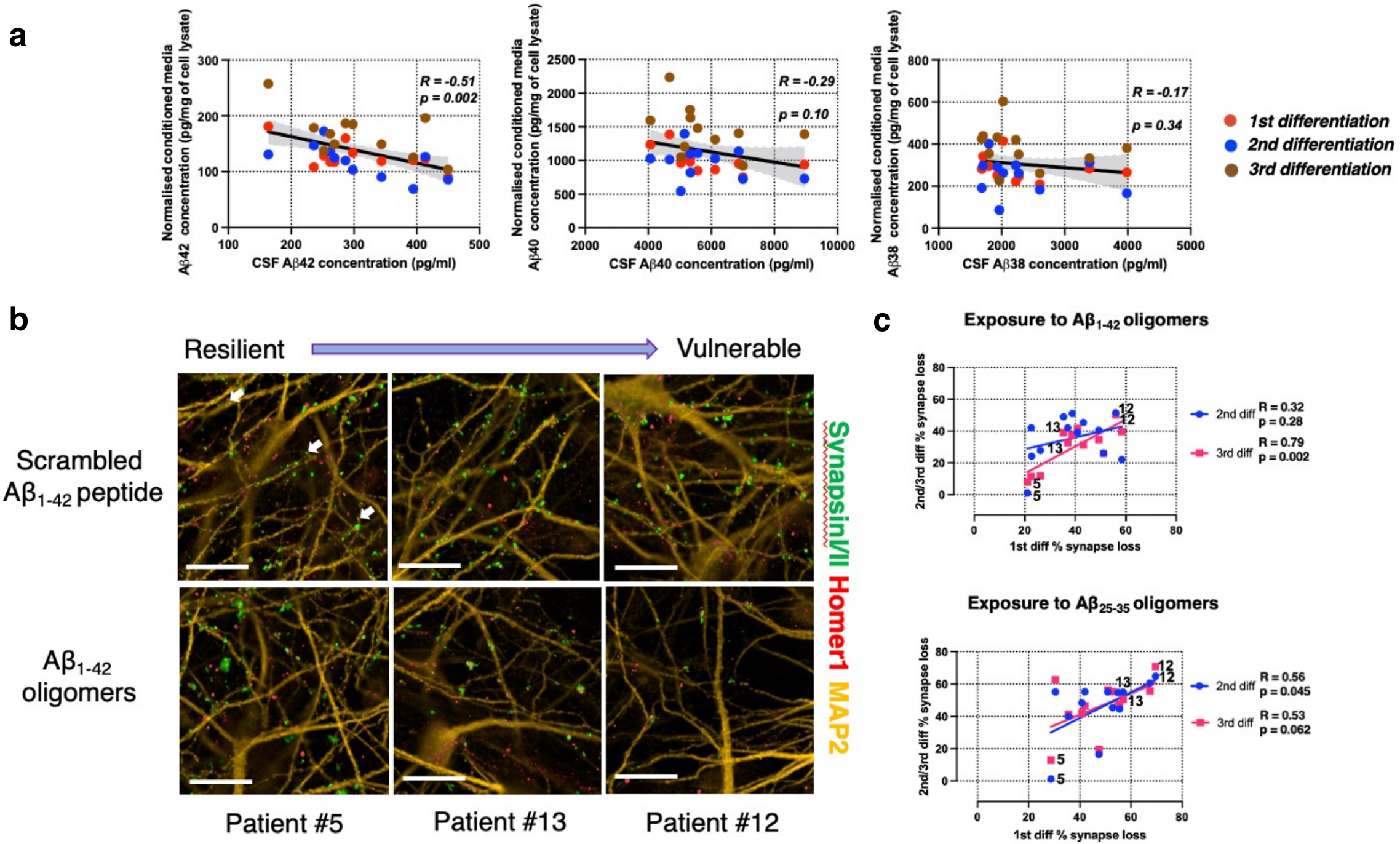
a
Normalised conditioned media Aβ42 concentration (pg/mg of cell lysate)
CSF Aβ42 concentration (pg/ml)
R = -0.51
p = 0.002
Normalised conditioned media Aβ40 concentration (pg/mg of cell lysate)
CSF Aβ40 concentration (pg/ml)
R = -0.29
p = 0.10
Normalised conditioned media Aβ38 concentration (pg/mg of cell lysate)
CSF Aβ38 concentration (pg/ml)
R = -0.17
p = 0.34
1st differentiation
2nd differentiation
3rd differentiation
b
Resilient
Vulnerable
Scrambled Aβ1-42 peptide
Aβ1-42 oligomers
Synapsin/Homer1 MAP2
Patient #5
Patient #13
Patient #12
c
Exposure to Aβ1-42 oligomers
2nd/3rd diff % synapse loss
1st diff % synapse loss
2nd diff R = 0.32 p = 0.28
3rd diff R = 0.79 p = 0.002
Exposure to Aβ25-35 oligomers
2nd diff R = 0.56 p = 0.045
3rd diff R = 0.53 p = 0.062

Fig. 1

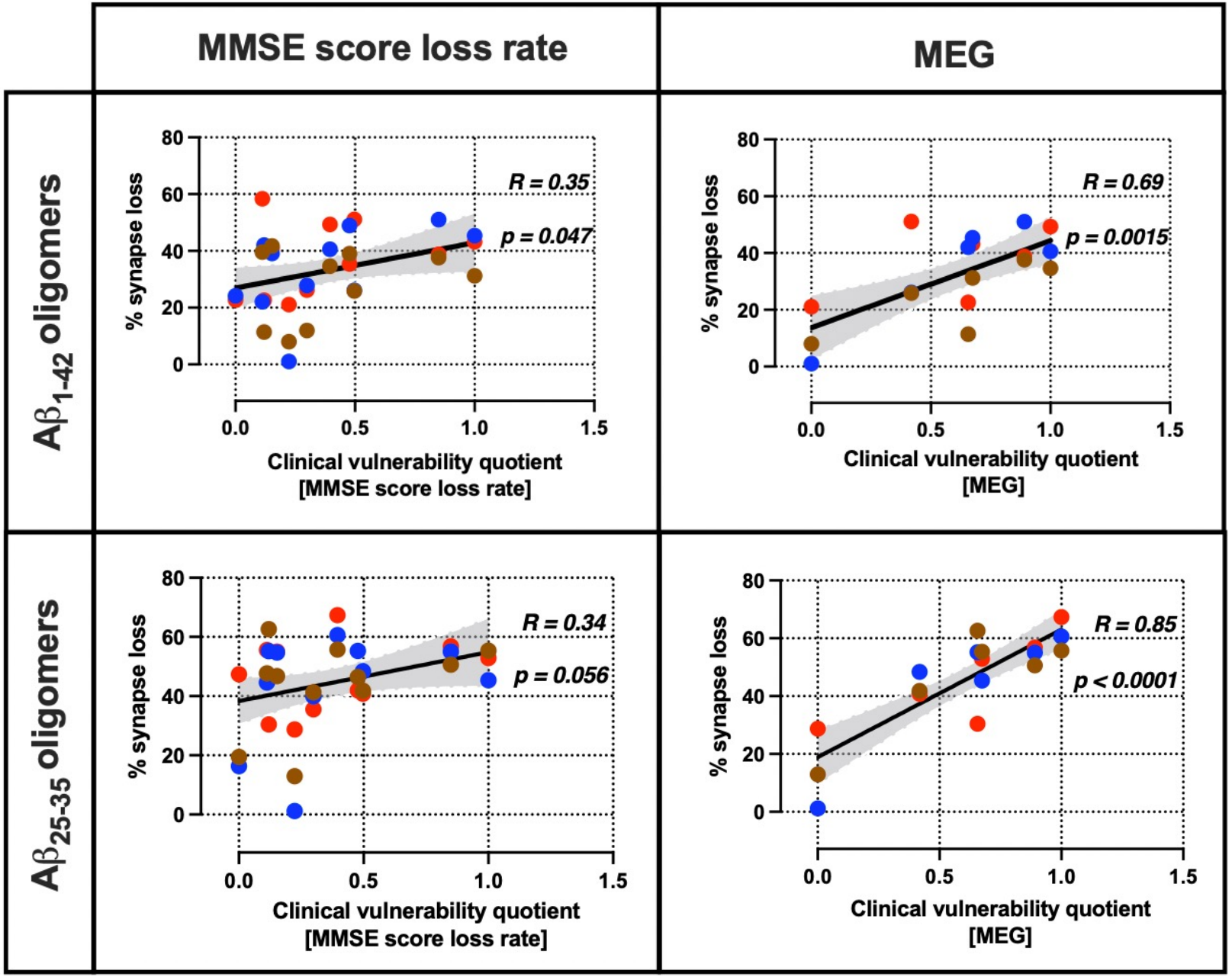
MMSE score loss rate
MEG
Aβ1-42 oligomers
Aβ25-35 oligomers
% synapse loss
Clinical vulnerability quotient
[MMSE score loss rate]
[MEG]
R = 0.35
p = 0.047
R = 0.69
p = 0.0015
R = 0.34
p = 0.056
R = 0.85
p < 0.0001
1st differentiation
2nd differentiation
3rd differentiation

Fig. 2

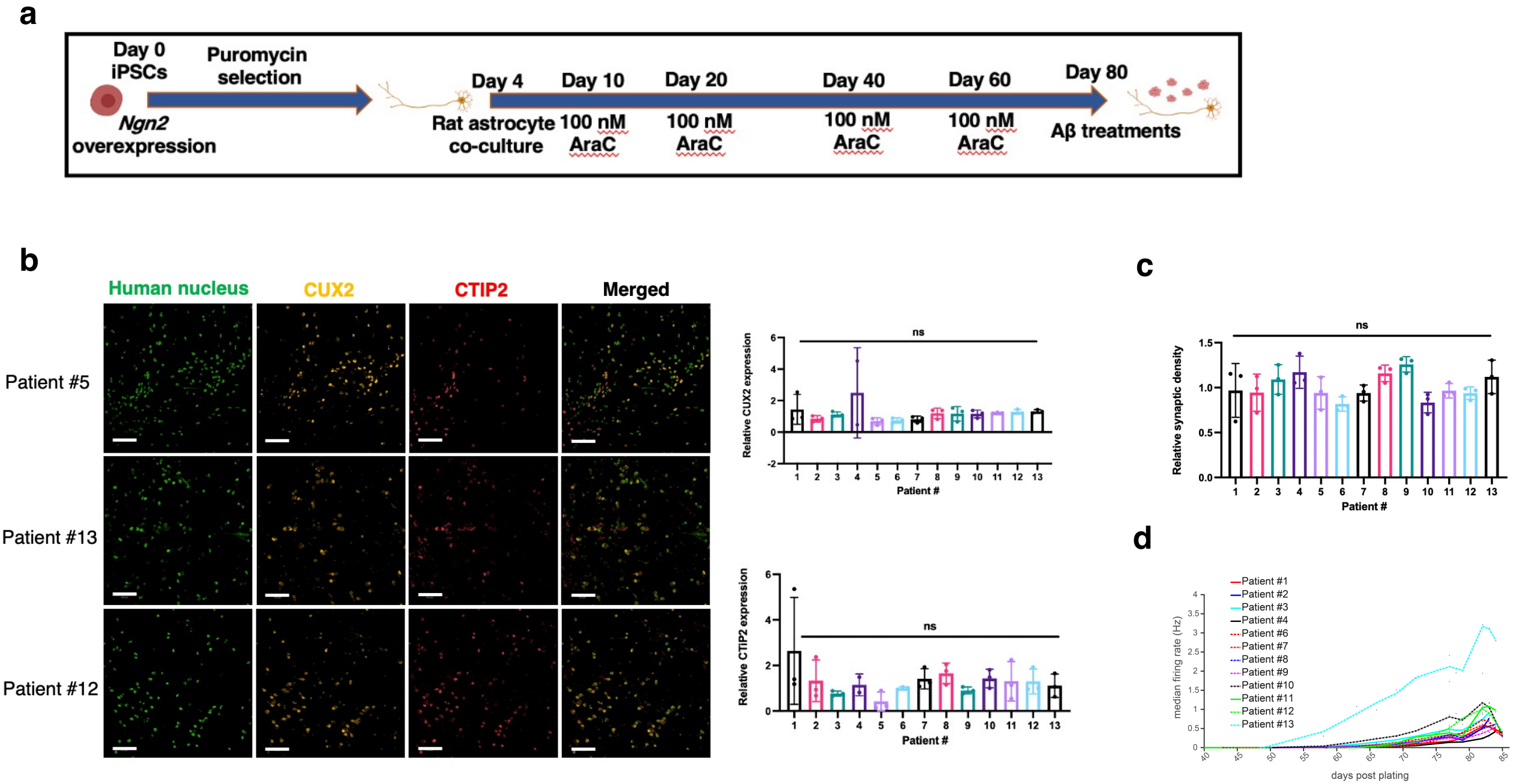

Extended Data Fig. 1

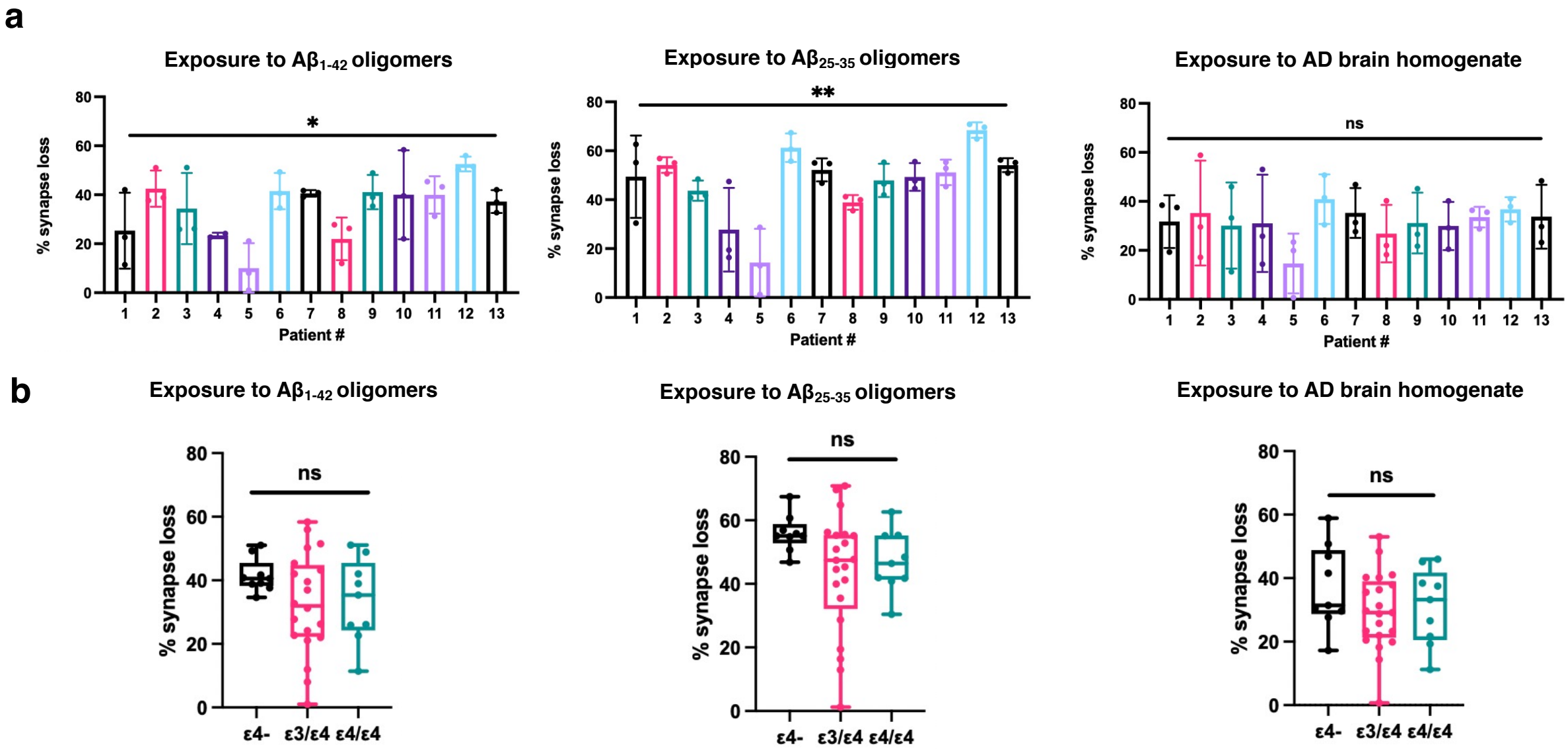

Extended Data Fig. 2

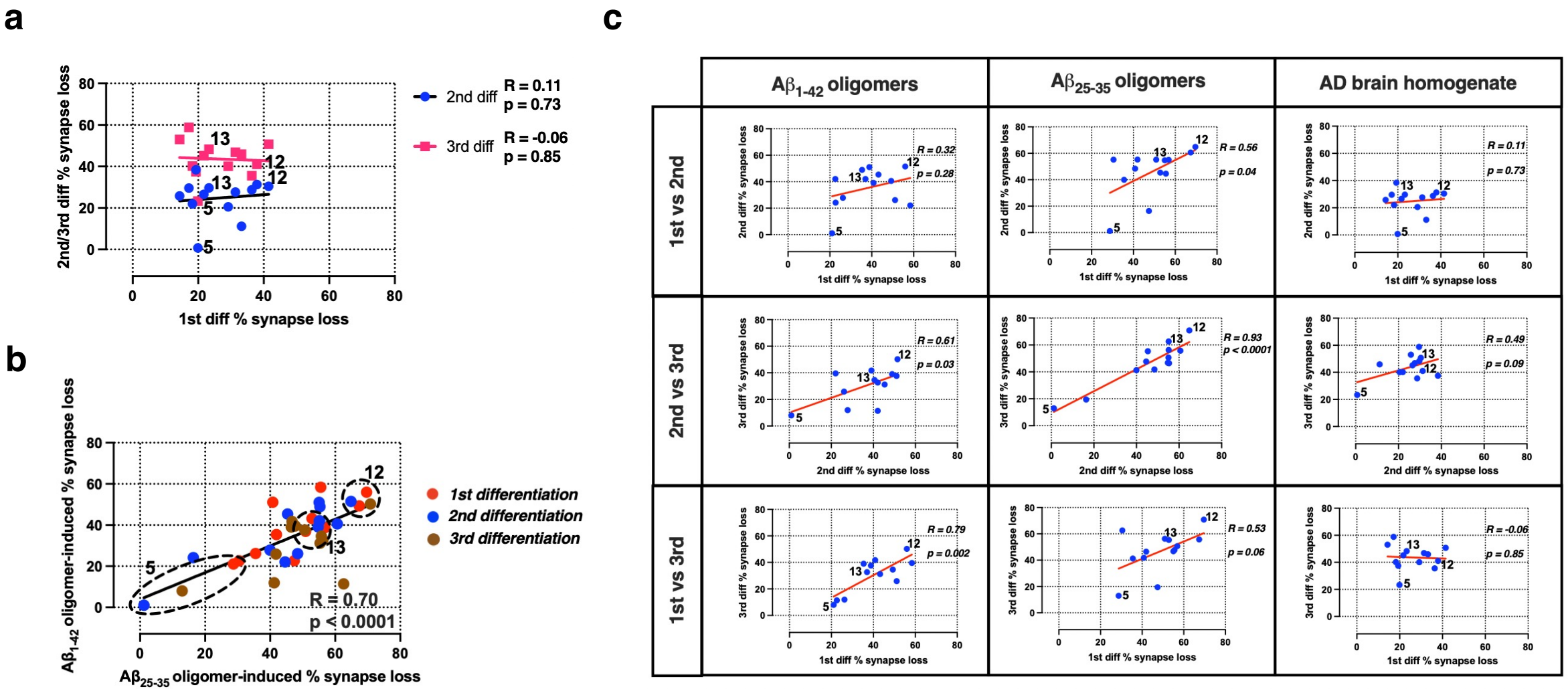

Extended Data Fig. 3

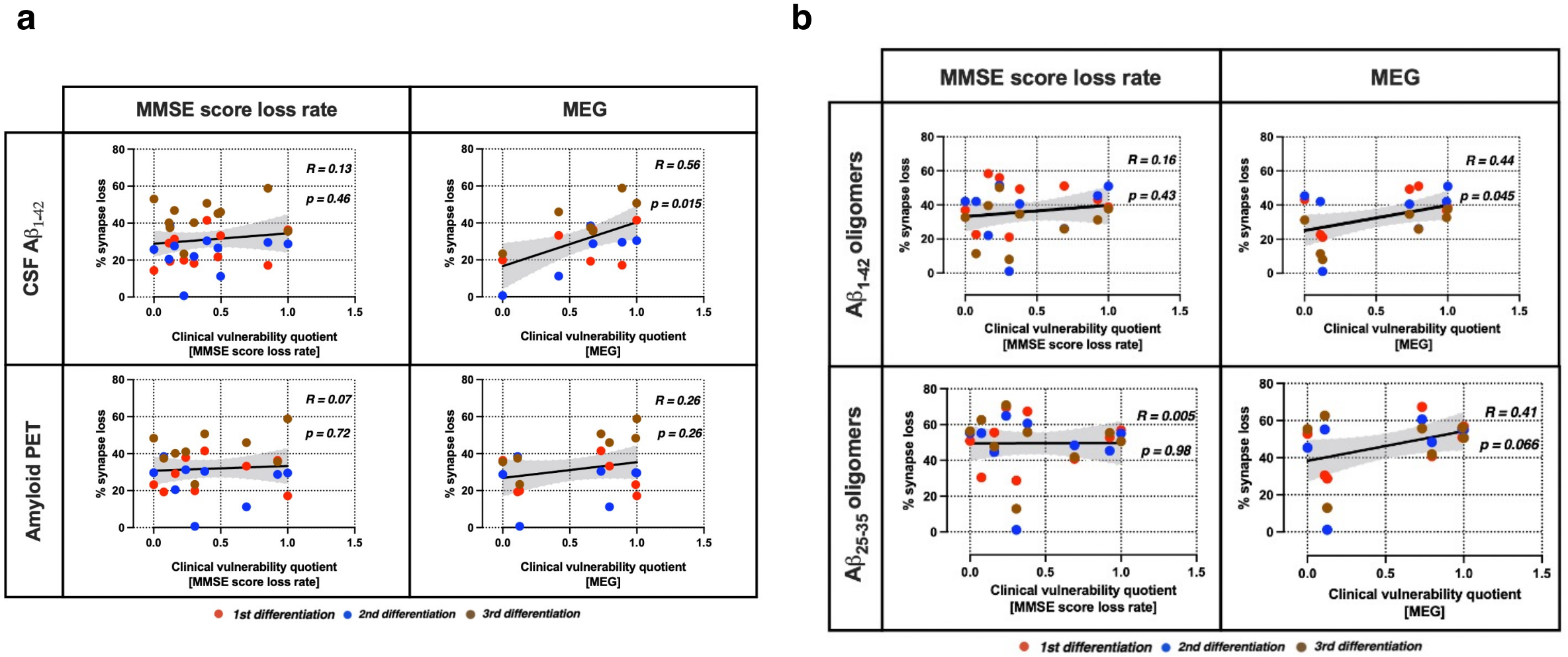

Extended Data Fig. 4

Supplementary Table 1: Characteristics of the Deep and Frequent Phenotyping pilot cohort patients

			AD biomarkers		Clinical outcomes	
Patients	*MMSE score*	*APOE genotype*	*Cortical amyloid PET (SUVR)*	*CSF $A\beta_{1-42}$ concentration[§] (pg/ml)*	*MMSE score loss rate[§§] (per day)*	*Global MEG recording[§§§]*
1	22	ε4/ε4	1.60	298	1.5×10^{-3}	0.974
2	24	ε2/ε3	1.21	269	8.4×10^{-3}	0.983
3	23	ε4/ε4	1.28	344	6.3×10^{-3}	0.985
4	27	ε3/ε4	N/A	395	0.2×10^{-3}	N/A
5	25	ε3/ε4	1.60	450	3.9×10^{-3}	0.979
6	22	ε3/ε3	1.28	252	3.7×10^{-3}	0.966
7	27	ε3/ε3	N/A	236	1.2×10^{-3}	N/A
8	29	ε3/ε4	N/A	262	3.0×10^{-3}	N/A
9	26	ε4/ε4	N/A	164	2.9×10^{-3}	N/A
10	24	ε3/ε4	1.30	414	1.9×10^{-3}	N/A
11	24	ε3/ε4	1.62	287	10.5×10^{-3}	0.944
12	26	ε3/ε4	1.56	N/A	3.1×10^{-3}	N/A
13	29	ε3/ε4	1.18	N/A	0.5×10^{-3}	0.961

[§] Average value between two visits which were 169 days apart

[§§] Derived from two MMSE measurements between the baseline visit and onset of symptoms

[§§§] Global efficiency metric from the γ-band (32-100 Hz)

Note: N/A – not available

Supplementary Table 2: DFP pilot cohort patient-derived iPSC IDs	
Patient #	**iPSC ID**
1	BPC-927 03-01
2	BPC-928 03-07
3	BPC-929 03-07
4	BPC-932 03-03
5	BPC-934 03-02
6	BPC-936 03-07
7	BPC-937 03-01
8	BPC-939 03-01
9	BPC-940 03-08
10	BPC-943 03-03
11	BPC-944 03-04-01A
12	BPC-946 04-10
13	BPC-947 04-09

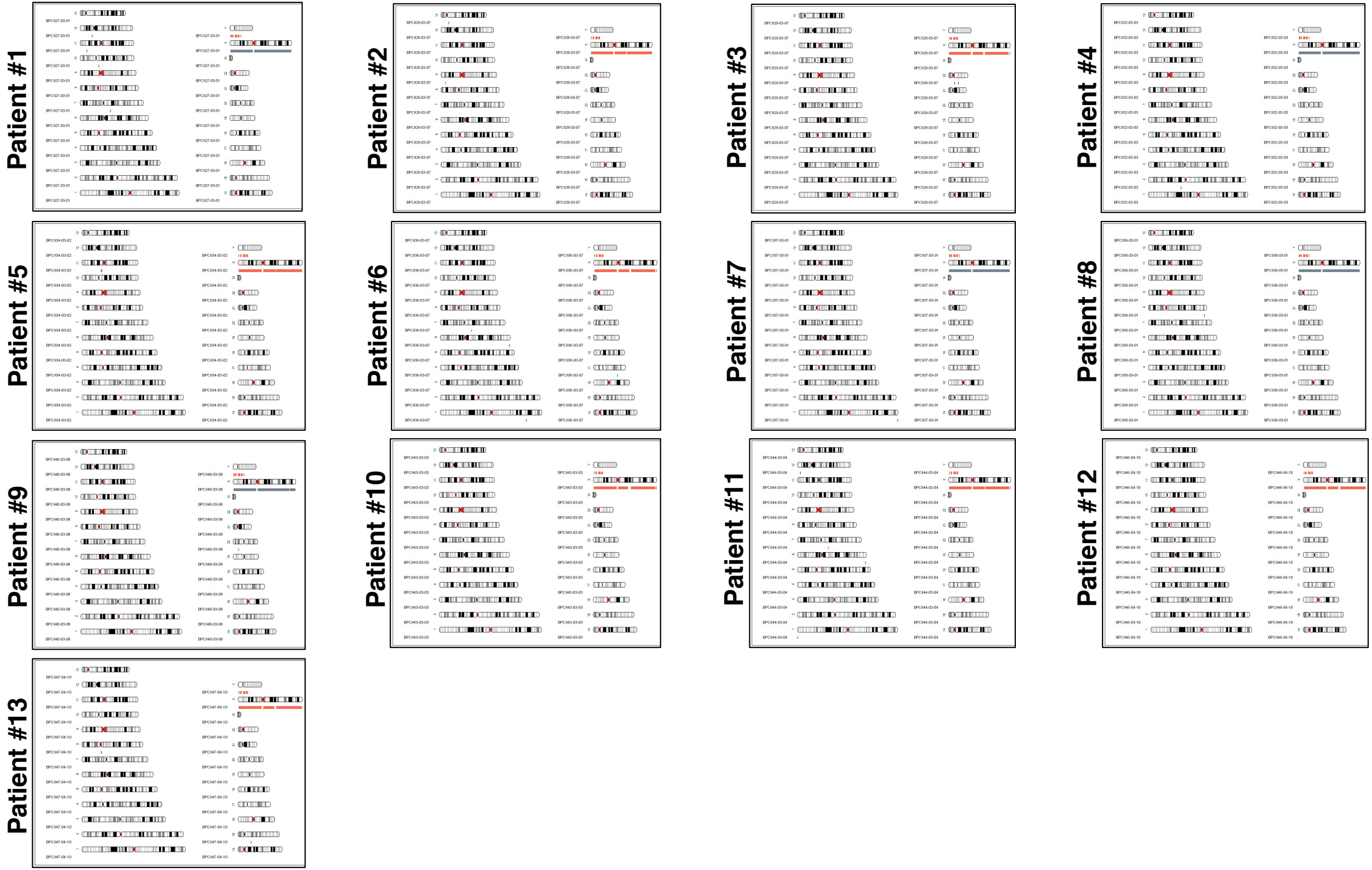
Patient #1
Patient #2
Patient #3
Patient #4
Patient #5
Patient #6
Patient #7
Patient #8
Patient #9
Patient #10
Patient #11
Patient #12
Patient #13

Supp. Fig. 1

Supplementary Figure 1: AD patient-derived iPSC quality controls.

Genome integrity of the AD patient-derived iPSC lines, examined by the Illumina OmniExpress24 SNP array. Karyograms (KaryoStudio, Illumina) show amplifications (green)/deletions (orange)/loss of heterozygosity regions (grey) alongside the relevant chromosome. Female X chromosome is annotated in grey.